Preferred citation: A. Madani, S. Storey, J.A. Olson, I.A. Frigaard, J. Salmela and D.M. Martinez. Novel fractionation methods: Separation in a viscoplastic fluid. In **Advances in Pulp and Paper Research, Oxford 2009**, *Trans. of the XIVth Fund. Res. Symp. Oxford, 2009*, (S.J. I'Anson, ed.), pp 19–49, FRC, Manchester, 2018. DOI: 10.15376/frc.2009.1.19.

NOVEL FRACTIONATION METHODS: SEPARATION IN A VISCOPLASTIC FLUID

A. Madani, S. Storey, J.A. Olson and I.A. Frigaard

Dept. of Mechanical Engineering
The University of British Columbia, 2324 Main Mall,
Vancouver BC, V6T 1Z4, Canada

J. Salmela

VTT, P.O. Box 1603, FIN-40101, Jyväskylä, Finland

D. M. Martinez

Dept. of Chemical and Biological Engineering,
The University of British Columbia, 2360 East Mall,
Vancouver, BC, V6T 1Z3, Canada

ABSTRACT

In this work we propose a novel separation technique based upon the control of the threshold for motion of different classes of particles in yield stress fluids. The principle is demonstrated by observing the motion of particles under the influence of a centrifugal force in a weak gel. Here we develop calibration curves of the force required to initiate motion in a gel under numerous configurations of the particles. Demonstration separations of bidisperse suspensions are reported. Here we achieve complete separation of dilute suspensions based upon length, diameter, or density.

1 INTRODUCTION

Fibre fractionation is the process of separating pulp fibres on the basis of their physical properties. The resulting pulp fractions can have significantly different papermaking quality. Papermakers fractionate to allow targeted processing of the low quality fraction to improve product performance while minimizing the amount of processing and subsequent energy, chemicals and capital required. The pulp fractions can also be used to produce papers with radically different properties. For example, fractionating the short fibre from the long fibre can create a short fibred paper that has excellent printing characteristics and a long fibred paper with high tensile strength. Further, the fibre fractions can be blended to create a spectrum of products designed for each of the many paper applications.

There are essentially two industrial methods to fractionate pulp fibres in use today: pressure screens and hydrocyclones. In pressure screens, the fibre suspension is fed into the annular gap between a rotor and an outer cylinder containing small apertures. The screen apertures are either narrow slots (as small as 0.1mm wide) or small diameter holes (as small as 0.8mm in diameter). The surface of the cylinder can either be smooth or be contoured. Separation here is based upon length as the small particles pass through the apertures. Several studies have been completed to understand how the operation and design of screens and screening systems affect fibre fractionation efficiency; general reviews of the topic are given by Sloane [1], Julien Saint Amand *et al.* [2] and by Olson and his co-workers [3–5].

With regards to the second fractionation method, there are a number of experimental studies that have shown that hydrocyclones are able to separate fibres based on its specific surface (fibre surface area per gram). This results in a separation of earlywood, large diameter thin walled fibres from latewood, small diameter, thick walled fibres, e.g, Paavilainen [6]. In addition, hardwood vessel elements have been shown to be effectively removed by hydrocylones. In a particularly interesting study by Vomhoff & Grundström [7] a chemical pulp was separated using a system of 5 hydrocyclone stages and the resulting two distinct fractions were refined separately and the quality determined. The one fraction contained 89% and the other 46% earlywood fibres, respectively. The unrefined fine fibre fraction was shown to have a tensile strength 3.5 times that of the coarse fibre fraction. After refining, the coarse fibre fraction tensile strength increased to that of the fine fibre fraction but required significantly more refining. This study indicates the industrial potential for fractionation based on cell wall thickness.

The efficiency for fractionation in both hydrocyclones and pressure screens is known to be relatively low. We feel that the inherent separation potential is

not realized because the complexity of the flow within theses devices. A stochastic element is introduced into the system through turbulence, the presence of boundaries, flocculation, and long range hydrodynamic interactions and these effects diminish the efficiency of the separation process. In this work we propose a new principle for fractionation and present a series of experiments demonstrating its utility. Here we show that fractionation can indeed proceed based on either length, diameter or density in a mechanistic fashion. In §2.1, the literature review, we present the background material leading up to this novel principle. Here we demonstrate first why separation with a Newtonian fluid is difficult (but not impossible) and then proceed to develop and justify the novel principle. In §3–4, simple demonstrations experiments highlighting this principle are described and the results discussed. The foreseeable limitations of this process are discussed in §5.

2 LITERATURE REVIEW

2.1 The underlying fractionation mechanism

Understanding the relative motion of particles in a flowing fibre suspension undergoing fractionation is difficult, if not impossible. Insight into this mechanism can by gained by examining the simplest case of the motion of an isolated particle, in an unbounded fluid, settling under the influence of gravity. An important case occurs when the particle is traveling at its steady terminal velocity u where the net weight of the particle is exactly counterbalanced by the drag force F_d, i.e.[1]

$$F_d = \Delta\rho V g \tag{1}$$

where V is the volume of the particle; $\Delta\rho = (\rho_p - \rho)$ is the difference in density between the particle ρ_p and the fluid ρ, and g is the acceleration due to gravity. If the drag coefficient C_d is defined as

$$C_d = \frac{2\,F_d}{\rho u^2 A} = \frac{2\Delta\rho V g}{\rho u^2 A} \tag{2}$$

and the inverse of the specific surface of the particle is assigned to be $\ell = V\rho_p/A$, Equation 2 can be rearranged to give

[1] In this simple example we assume that the particle does not rotate nor drift from the gravity direction. We do so for clarity in the presentation and this assumption does not distract from the main point of this simple example.

$$u^2 C_d = 2\ell g(\frac{\Delta\rho}{\rho\rho_p}) \tag{3}$$

This indicates that the terminal velocity is proportional to the specific surface of the particle and strongly supports the fractionation mechanism advanced by Paavilainen [6].

The equation derived above applies for all classes of particles. We can gain further insight into the fractionation process by examining one class of particles in which a closed form analytical expression can be derived for the drag coefficient. This is the case of cylindrical particles settling under creeping flow conditions, that is at $Re \to 0$, where Re is the Reynolds number based upon the length of the fibre. This work was performed originally by Batchelor [8], and subsequently extended by Mackaplow & Shaqfeh [9], and indicates that the terminal velocity is given by a function of the form

$$\boldsymbol{u} = \frac{\Delta\rho d_f^2}{16\mu}[(\ln 2r + 0.193 + O(\ln 2r)^{-1})\boldsymbol{g} + (\ln 2r - 1.807 + O(\ln 2r)^{-1})(\boldsymbol{p}\cdot\boldsymbol{g})\boldsymbol{p}] \tag{4}$$

where r is the aspect ratio of the fibre defined by L/D; μ is the viscosity of the fluid; and $\boldsymbol{p}$ is a unit vector that indicates fibre orientation. The **bold** font indicates a vector quantity. This equation implies that unlike spheres, fibres can have significant motion perpendicular to gravity; the drift velocity is strongly dependent upon its orientation. Jayaweera & Mason [10] indicate that with $Re < 0.01$, cylinders do not tend to rotate during settling – they tended to fall in the same attitude with which they were released. The key finding here is that for cylindrical particles, the terminal velocity is not a unique value based upon the properties of the particles; it is also related to the aspect ratio and orientation of the cylinder. With these findings, one can argue that a mechanistic means of separating particles exists. Under more realistic conditions, i.e. at elevated concentrations and Reynolds numbers, disturbances must be introduced into the suspension which would result in a distribution in the terminal velocity. We shall consider two classes of disturbances below and characterize the resulting distributions in the terminal velocity.

In the first case, category 1, we consider disturbances in the suspension created by the presence of other particles. The concentration of the fibre suspension need not to be large and we restrict our argument to the influence of the "wake" of one particle moving in the vicinity of another. This phenomenon is not new. With swarms of settling particles Happel & Brenner [11]

explain that the physics becomes more complex as each individual fibre settles and rotates under the influence of the "wakes" or "long-range hydrodynamic disturbances" of the other settling particles. This leads to inhomogeneous settling rates and local floc formation. With monodisperse glass fibre suspensions, floc formation has been observed by Kumar & Ramarao [12] who noted that as the fibre concentration increased, the number of flocs increased and caused greater hindrance effects. To help understand this behavior, Herzhaft & Guazzelli [13] visualized the motion of marked glass fibres, in a suspension of unmarked fibres made optically transparent by matching the index-of-refraction. By doing so, they were able to measure both the velocity and orientation of a particle. They found that in the dilute regime, the ensemble-averaged settling velocity *actually increases* with concentration and *may exceed* the velocity of an isolated particle. They also observed that under these conditions most of the fibres were aligned in the direction of gravity. In the semi-dilute regime, however, the sedimentation velocity decreased according to the Richardson-Zaki correlation [14]. There are only a few numerical simulations available in the literature which attempt to describe this process under these conditions [9, 15, 16]. In general these works were conducted in the limit of $Re \rightarrow 0$, using slender body theory, and suggest that the settling suspension should segregate into particle clumps. Koch & Shaqfeh [16] were the first to describe an instability mechanism that leads to floc formation. They advanced an argument that a 'test' fiber in the velocity field far from a sedimenting single fiber tends to orient its main axis such that the relative velocity of the two particles became negative. Thus, the particles will tend to form clusters until near-field effects or contact forces intervene. Mackaplow & Shaqfeh [9] present two results using (i) Monte-Carlo simulations of static fibre assemblies and (ii) point-particle approximations for the dynamic case. They observed fibre clustering and velocities greater than that of an isolated particle. Steady state, however, was not reached by the end of the simulations. Butler & Shaqfeh [15] simulated the motion of swarms of particles in the limit of zero Reynolds numbers using slender-body theory. They observed fibre clustering and a fibre rich stream in the middle of the computational domain. Their simulations were in good agreement with experimental results of Herzhaft & Guazzelli [13].

We continue this discussion by considering the second category of disturbances which are created at elevated Reynolds numbers. Our attention is focussed on this regime as this *Re* range represents the range relevant for papermaking fibres settling in water [17]. It has been shown that, unlike in the Stokes' regime, at Reynolds numbers $Re \sim O(1)$ isolated non-spherical particles tend to exhibit preferential orientation during settling. At these Reynolds numbers, in the dilute limit many investigations have shown that

isolated non-spherical particles tend to exhibit *preferential orientation* during settling [10, 18, 19]. The torque induced on thin cylinders causes the body to rotate into a stable position with its symmetry axis aligned horizontally. Feng, Hu & Joseph [18] show that particles migrate towards the center of the channel due to wall effects. At elevated concentrations, the long range hydrodynamic interactions perturb the flow field to the point where recirculation or swirling like structures are apparent [20]. A representative case displaying this phenomenon is given in Figure 1. The result was visualized using particle image velocimetry, a common flow visualization method, and is reported at four different times. The initial concentration of the suspension in this case was 0.3% (vol/vol); this is equivalent to a crowding number of $N = 5$ which represents roughly handsheet concentrations. What is clear in Figure 1 is that the particles recirculate while settling. Clearly, this indicates that the terminal velocity is not a unique value as this stochastic swirl is superimposed on the settling motion. In later work Salmela *et al.* [21] completed a more comprehensive study using a similar index-of refraction matching technique and studied the motion of settling particles as a function of concentration, aspect ratio, fluid viscosity, and fibre length for both monodisperse and bidisperse suspensions. What sets this work apart is that the motion of tracer fibres could be tracked three-dimensionally; hence fibre fractionation could be studied in this equipment. Like Herzhaft & Guazzelli [13], Salmela *et al.* [21] reported non-monotonic behaviour in the average settling velocity as a function of concentration with the maximum velocity occurring at a volume fraction of $\phi = 0.05\%$. With papermaking fibres, non-monotonic behaviour has also been observed with the maximum in the initial settling speed occuring at a crowding number of $N \sim 16$ [20]. Salmela *et al.* [21] also indicated that the orientation state of the suspension also displayed complex behaviour under these conditions. They report that the suspension was preferentially oriented in the horizontal state at low concentrations and then adopted an increasing proportion of fibres in the vertical state as concentration increased.

We now turn to what we consider the key findings from unpublished results of Salmela and his coworkers which sheds light onto the mechanistic understanding of the ability to fractionate based upon settling. Although not reported in [21], the results stem from this study. Here they examine the motion of a bidispersed suspension comprised of glass rods of two different aspect ratios $r = 23$ and 50 and measured the ensemble-averaged settling velocity of each class of particle. These authors measured this as a function of the initial suspension concentration, see Figure 2. Here the results have been made dimensionless by scaling with the average of the isolated velocity of the two different particles settling in the vertical position; these values were determined by experiment. What is clear from this figure is that under dilute

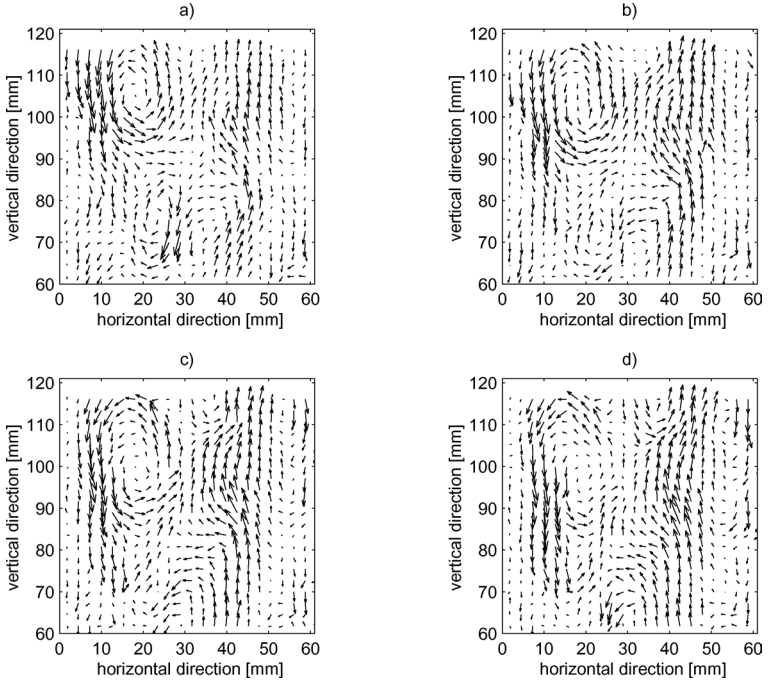

Figure 1. The motion of index of refraction matched 5mm in length glass fibre suspension settling in a viscous fluid [20].

conditions each fibre fraction settles at statistically different velocities. In this region fractionation may be possible. With increasing concentration, the differences between the terminal velocities diminish until their difference is indistinguishable.

To summarize the existing literature, we find that for isolated particles in an unbounded fluid the terminal velocity is related to the density, diameter, aspect ratio and orientation of the cylinder. Under creeping flow conditions with extremely dilute suspensions, we can draw the conclusion that we can indeed separate fibres based upon the terminal velocity, if and only if, the orientation distribution remains constant during descent. We find that at elevated concentrations, for all *Re* above the creeping flow conditions, long range hydrodynamic disturbances lead to floc formation and swirling chaotic structures. Salmela *et al.* [21] have shown that there is no statistical difference between the terminal velocity at any reasonable concentration. This present study is motivated from these findings.

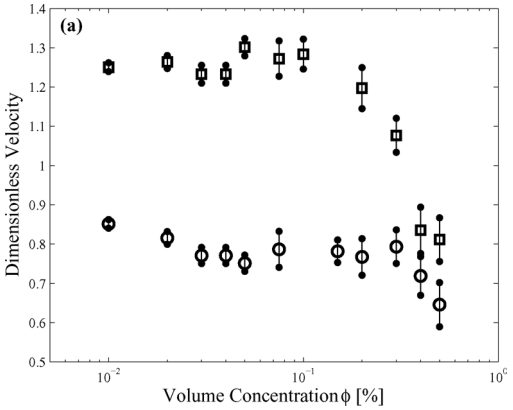

Figure 2. Dimensionless mean settling velocity versus volume concentration ϕ for a bidispersed suspension comprised of equal masses of particles with aspect ratios of $r = 50\%$ (□) and $r = 23\%$ (○). The uncertainty in the estimate is reported as the 95% confidence interval. The Reynolds number in this case based upon the average fibre length was estimated to be $Re \approx 0.12$.

2.2 Hydrodynamics of a hydrocyclone

With this understanding of how particle suspensions move in simple flow field, we attempt to describe the flow field that occurs in a hydrocyclone. Clearly the flow field in the hydrocyclone is three dimensional, i.e. there are three components of flow which vary both in the radial and axial directions. At long-time scales the flow is considered axi-symmetric, i.e. the order of magnitude of the radial and axial flows must be similar; the swirl or tangential flow is the dominant flow component in this device. The salient point here is that the flow is quite complicated in the inlet region and with certain devices flow reversal occurs in the central core of the hydrocyclone. Further details of this flow field are given by Ko [22], Narashima *et al.* [23], and Nowakowski & Dyakowski, [24] and the references contained therein.

In perhaps the most relevant work in the this area is that by Bergstrom & Vomhoff [25]. Here they map out the flow field in cylindrically shaped hydrocyclone using both a pitot tube to measure the tangential component and ultrasound velocimetry to measure the radial component. With regards to the tangential body, these authors report that under dilute conditions the flow field observed resembles quite closely to a combination of free and forced vorticies. At higher conditions, namely after 7.5 g/L mechanical

entanglement dominates and creates a flow field which resembles solid body rotation.

A number of research groups, Hsieh & Rajamani [26] and Sevilla & Branion [27], have attempted to predict particle trajectories in these devices under extremely dilute conditions. These models are generally considered to be coupled "one-way", i.e. the fluid affects the particle motion and not the other way around. Expressions for radial movement of particle was obtained by balancing the centrifugal force with the radial component of the drag force; this form of balance equation is very similar to that considered for the settling isolated particle described in the previous section. Similarly, for particle motion in axial direction, these authors equate the gravity force with the axial drag force. Boysan *et al.* [28] and Ma *et al.* [29] determined the particle drag force and used it in a stochastic particle tracking technique. In their method, they did not consider the velocity fluctuation due to turbulence while formulating the drag force equation. A discrepancy was noticed between the behaviors of small particles when compared to experimental results.

What is clear in this body of literature is that the tangential flow creates a centrifugal force which causes particle migration in the radial direction. For the residence time of the fibre in this device, the separation efficiency is largely dependent upon the ability of the particle to migrate in the radial direction. In the previous section, we advanced the argument that the terminal velocity of an isolated particle is not the sole indicator of the ability to migrate. The mobility of the fibre is also a function of long range hydrodynamic disturbances and flocculation. The flow field in the hydrocyclone is turbulent and this too will hinder particle migration and diminish the separation efficiency.

2.3 Towards a novel fractionation principle

From the above review we see that the motion of a particle suspension at any industrially relevant concentration and Reynolds numbers is extremely complex. Chaotic behavior is evident due to long-range hydrodynamic interactions. Since these observations were made under ideal settling conditions, we anticipate an even richer behavior to occur in the complex three-dimensional, time-dependent, turbulent flow fields encountered in industrial hydrocyclones. As a result, instead of trying to improve an already complex coupled fluid-fibre interaction problem, we are attempting to devise a new separation principle which is not hindered by long-range disturbances. We feel that this may be achieved through use of a yield stress fluid[2].

[2] Everyday examples of yield stress fluids are Ketchup, Mayonnaise, and salad dressing. With these fluids, the yield stress is the applied stress that must exceeded in order to make the fluid flow. Ketchup has a yield stress of approximately 15 *Pa*.

To introduce our novel fractionation principle we consider once again the illustrative problem of an isolated particle settling in a yield stress fluid. With yield stress fluids, the settling problem is more complex: the presence of a yield stress implies that settling can only occur if the net applied force F_a is greater than the resistive force due to the yield stress of the material. Despite the simplicity of the problem, the mechanism by which the particle settles is poorly understood. Clearly a critical force is required to initiate the motion of the particle. To highlight this, consider as an example a particle immersed in a material having a yield stress τ_y. If F_a is not sufficient to overcome the yield stress then the object will be suspended indefinitely. Motion will commence when

$$F_a > \tau_y A_e \tag{5}$$

where A_e is the surface area over which the force is applied. The exact value for A_e however remains an open question. The above relationship can be made dimensionless by scaling each side by a characteristic area of the particle. In this case if we divide each side of the equation by D^2, we can define a dimensionless force ratio F which represents the criteria for motion

$$F = \frac{F_a}{\tau_y D^2} > \frac{A_e}{D^2} \tag{6}$$

The bound where motion begins is defined as the critical force ratio F_c.

The key to the separation is the determination of A_e. A number of researchers have attempted to determine A_e through simulation and we divide the methods into four groups. In the first category are estimates made through an assumption regarding the shape of A_e. For example, through a simple force balance Andres [30] argues that for spherical particles A_e is related to the projected area of the particles and reports that motion should commence when $F_c = 4.8$. In the second category are regularization models in which a continuous function is used to approximate the rheological behavior of the yield stress fluid [31–34]. In essence this approach avoids the singularity inherent with strain rate decreasing to zero in unyielded regions. A detailed review of this approach is given in Frigaard & Nouar [35]. The third category of methods involves domain mapping. In this category falls the work of Beris *et al.* [36], which we consider to be the benchmark paper in this area. Combining a regularized model with an intricate mapping of the yield surfaces onto a standard domain, they were able to calculate the position of the yield surface of a settling sphere very accurately for one class of yield

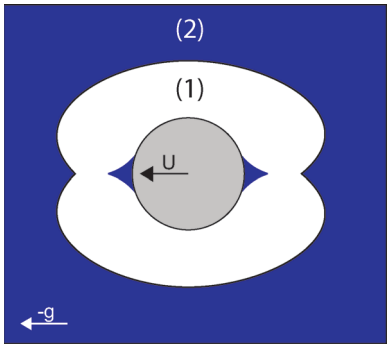

Figure 3. Schematic illustrating the yielded (region (1)-white) and unyielded flow regions (region (2)-blue), according to the numerical results by Beris *et al.* [36]. This figure was reproduced from Putz *et al.* [37].

stress fluids, that is a Bingham plastic[3]. By doing so they argue that two yield surfaces are evident: a kidney shaped surface in the far field and two somewhat triangular-cusps attached to the leading and trailing edges of sphere (Figure 3). With this, these authors indicate that particle motion would commence when

$$F_c = \frac{V\Delta\rho g}{\tau_y D^2} \approx \frac{7\pi}{2} \approx 11 \qquad (7)$$

This expression is approximately 3 times greater than that given by Andres [30] and are closer in magnitude to the experimental measurements of Tabuteau *et al.* [38], Attapatu *et al.* [45], Jossic & Magnin [46], and Laxton & Berg [39], i.e. $16 < F_c < 25$. The discrepancy in these estimates must stem from the approaches used: a perfect yield stress fluid is *assumed* in the theoretical treatments, i.e. this doesn't exist in reality; the experimental estimates are made from indirect measurements through extrapolation from slowly translating spheres. Here the yielding question is ill-defined. In the fourth category are simulations conducted using Augmented Lagrangian schemes [40, 41]. Roquet & Saramito [42] combined the augmented Lagrangian method with anisotropic grid refinement to obtain very accurate numerical results and have applied this method successfully to the flow around settling cylinders.

[3] A Bingham plastic is a viscoplastic material that behaves as a rigid body at low stresses but flows as a viscous fluid at high stress. When flowing, there is a linear relationship between the applied stress and the strain rate.

We now turn our attention to the experimental literature. An extensive summary of settling and sedimentation experiments in different media, including viscoplastic fluids, can be found in the book by Chhabra [43]. This review was published in 2007 and focuses generally on the calculation of the drag coefficient and the terminal velocity, i.e. engineering properties useful for design purposes. Recently there has been renewed interest in this problem due to the availability of (digital) particle image analysis (PIV). Gueslin, Talini, Herzhaft, Peysson & Allain [44], for example, used this technique to measure the flow field of a spherical particle settling in Laponite, an extremely thixotropic yield stress fluid. The objective of this work was to study the aging properties of this fluid. Putz *et al.* [37] experimentally estimated A_e through flow visualization experiments for two different size spheres settling in Carbopol solutions. Their results indicate that the shape of the yield surface approximates that of an ovoid spheroid with its major axis approximately 5 times greater than the radius of the particle.

To summarize, what is clear from this body of work is that during settling the flow is confined in the vicinity of the particle within an envelope the size of which is related to the yield stress of the material. For particles to settle, a critical force must be applied to overcome the resistance created by the yield stress. Relatively little is known about the shape of this surface and the magnitude of the applied force to create motion. What can be said is that the unyielded envelope is larger than the body itself but its shape has yet to be determined rigorously.

What is key in this description is that the differences in stability of particles in a yield stress fluid, under the influence of an applied force, may represent a novel criterion for separation. We expand upon this idea to highlight the principle. In this example, consider two different particles of equal dimensions but of different densities. Each particle is spun in a centrifuge at exactly the same angular velocity and at equal radial positions from the axis of rotation. In other words they experience the same acceleration field. The particle with greater density, however, experiences a larger centrifugal force as it has a larger mass. If we apply Equation 5, we see that separation of these two particles will occur if $F_{a1} > \tau_y A_e > F_{a2}$, where F_{a1} and F_{a2} are the centrifugal forces applied to each particle. This simple example leads us to the question: can we choose an applied force and a yield stress in which separation of particles is achieved? In this work we will attempt to address this question and devise simple experiments to illustrate this principle.

3 EXPERIMENTAL DETAILS

In this work we measure the critical force required to initiate motion of a particle in a yield stress fluid under the action of a centrifugal force. Two different centrifuges were used depending upon the force required. For low rotational speed experiments an in-house centrifuge was built. In this case, the centrifuge, which was made from plexiglass, was 250 *cm* in diameter, and 5 *cm* thick and was driven by a motor and controller, with a precision of 5 *rpm*, up to a maximum of rotational rate of 300 *rpm*. High speed experiments were conducted in a Universal Model UV centrifuge at rotational rates of up to 3000 *rpm*.

The main fluid used in this study was Carbopol-940 obtained from Noveon. In most of the work a 0.16% (wt/wt) solution was prepared using DI water and then neutralized using a dilute *NaOH* solution. The density of the resulting solution was that of water. The resulting gels were degassed and then allowed to rest overnight. Rheological characterizations were performed at room temperature in a cone and plate flow geometry on a Bohlin rheometer. Shear sweeps were performed in controlled strain mode typically in the range of 1×10^{-2} s^{-1} to 1 s^{-1} in order to determine the yield stress, a typical rheogram is shown in Figure 4(a) and the yield stress was estimated at the maximum of the curve shown in Figure 4(b). Here the uncertainty in the estimate can be as high as 100%. This is typical of most reported estimates for this parameter.

A number of different studies were performed in which density, diameter, aspect ratio, shape (degree of curl) of cylindrical rods were employed. Both rigid and flexible rods were considered. In our initial study, spherical particles were under the conditions outlined in Table 1 (shown in §A). Here particles were placed in the low speed centrifuge at a radial distance R from the axis of rotation and then spun at a fixed angular velocity ω for approximately 5 minutes. At the end of the experiment, the position of the sphere was inspected and if stable, the test was repeated by increasing the speed of the centrifuge. The procedure continued until motion was induced. With this the critical force ratio to induce motion was estimated using the following expression

$$F_c = \frac{\Delta\rho V R\omega^2}{\tau_y D^2} \tag{8}$$

It should be noted that the Carbopol solution was pretreated before data collection by allowing a number of spheres to settle in the solution. Both Attapatu *et al.* [45] and Putz *et al.* [37] indicate that reproducible settling

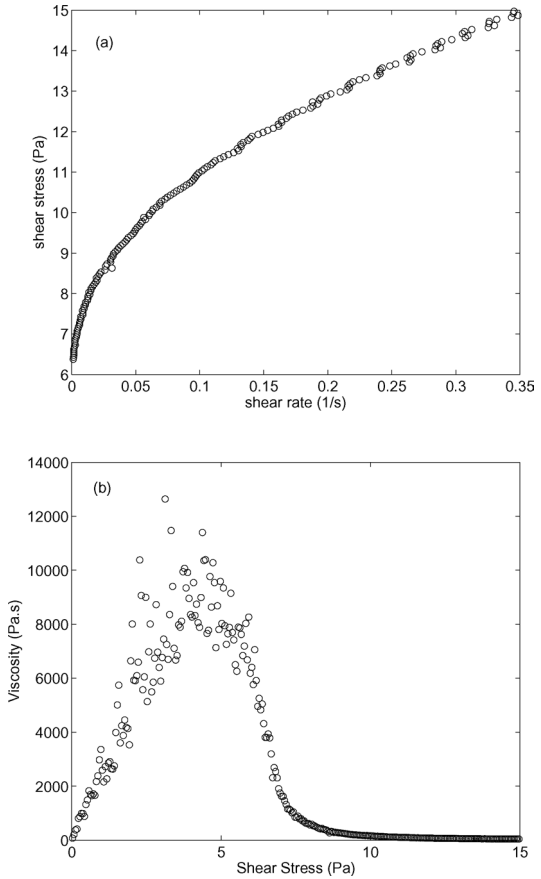

Figure 4. (a) A typical rheogram of shear stress versus shear rate for a 0.16% Carbopol solution. The local viscosity versus the shear stress for the same solution is given in (b). The yield stress is given at the maximum in this curve.

experiments can be obtained if approximately 4–5 spheres are allowed to settle in the gel.

In the second series of experiments we examine the stability of cylinders. In Tables 2–5 (see §A) a large series of experiments were conducted to measure F_c as a function of the density and aspect ratio L/D of the rod, the angle of orientation (relative to the direction of motion), and its shape, that is the degree of kink reported as S/L. S/L is defined as the end-to-end length S divided by the length of the rod. In these studies, the orientation is defined by

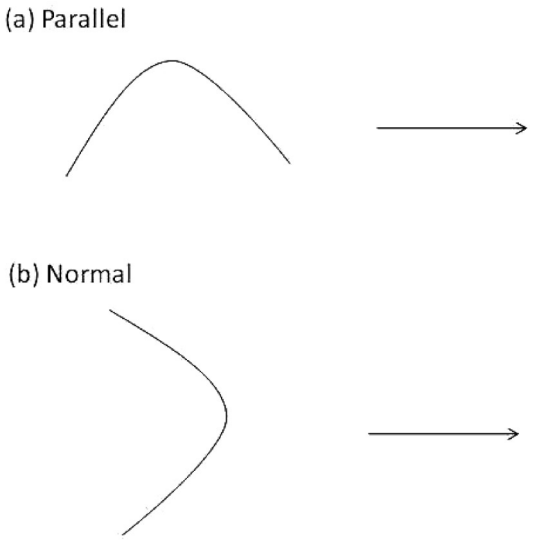

Figure 5. Schematic illustration of the orientation of bent rods used in the device. We define "parallel" to indicate the direction of the chord between the ends of the fibre make in relation to the direction of motion. In (a), we see that this is parallel to the direction of motion. In (b), the orientation is perpendicular to the direction of the applied force.

the direction of the chord connecting the two ends of the rod relative to the direction that the force is being applied. For the bent fibres as this is difficult to visualize so a schematic of this is shown in Figure 5.

4 RESULTS AND DISCUSSION

4.1 Spheres

Before proceeding to present the main findings of this section, it is instructive to examine the histograms of one test. As shown in Tables 1–5, a large number of tests were conducted for each experimental condition from which we could develop both a histogram and a cumulative probability distribution. A typical example of this is shown in Figure 6 where the histogram is smooth and clustered around a definite value. The cumulative distribution represents the fraction of particles which have remained unstable. In this case the

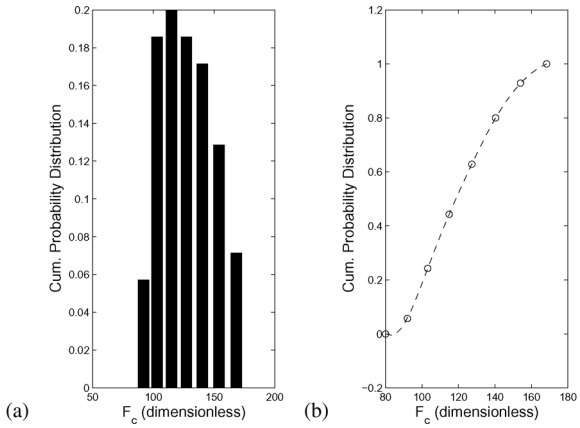

Figure 6. The histogram (a) and the cumulative probability distribution (b) for F_c measured on a 1.6 *mm* diameter and 2.54 *mm* length cylinder having a density of 7800 kg/m^3 with a fluid having a yield stress of 4 *Pa*. Approximately 70 observations were made. Cylinder axis of symmetry is parallel to the direction of motion.

histogram was skewed towards the lower values of F_c and this finding is representative of all cases tested. The critical values for each experiment are given in these tables in which the uncertainty in the mean is reported at the 95% confidence interval. What is evident is that motion occurs over a range of F_c and variation (standard deviation) in this estimate is typically 21% of the mean.

At this point we turn our attention to the estimates of F_c measured as a function of particle diameter, see Figure 7. The first observation that can be made from this figure is that F_c is a strong function of D. We consider this finding quite surprising as there is no indication of this in the literature. When we re-examine the pertinent works in the literature, i.e. Attapatu *et al.* [45] and Jossic & Magnin [46], we conclude that previously reported results were obtained from indirect methods; F_c was determined by extrapolation from measurements of a slowly translating sphere. The question of "slip" on the surface of the particle was not addressed in this work whilst making this extrapolation. In addition the uncertainty in the estimates given by Attapatu *et al.* [45] and Jossic & Magnin [46] are within the range of variation given in Figure 7. From this we conclude that the methods used in the previous literature studies were not sensitive enough to observe this functional relationship. Like Putz *et al.* [37] we too must draw the conclusion that the unyielded envelope is not spherical in shape (otherwise it would be independent of D).

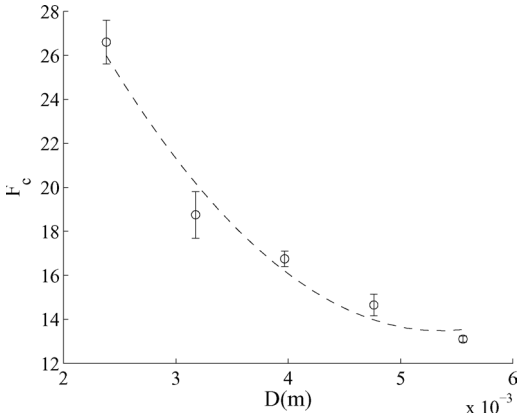

Figure 7. Estimate of the critical force required to initiate motion for stainless steel spheres with diameters in the range 2.4 $mm \leq D \leq 5.6$ mm.

At this point we turn to the main point of this section and we attempt to demonstrate the fractionation principle using one specific example. Here we create a separation based upon the differences in densities of two spheres having equal diameter. The spheres are placed in a centrifuge at equal radial distances from the axis of rotation and the angular velocity is set. From this we can estimate the force ratio F_1 and F_2 acting on each particle during the experiment. Three different scenarios can be constructed:

1. Both F_1 and F_2 are *less* than the critical force F_c determined in Figure 7. In this case both particles remain stably trapped.
2. Both F_1 and F_2 are *greater* than the critical force F_c. Here motion begins for both particles.
3. If $F_1 > F_c > F_2$, particle 2 remains stably trapped whilse particle 1 moves. Under this case separation has occurred. This is the separation principle

To highlight this last scenario we examine Figure 8(a) where we have created a bidisperse suspension of spheres with similar diameters but vastly different densities. The sphere with the larger density is shown in black and that with the smaller density in red. An equal number of each type of sphere is distributed throughout the centrifuge. If centrifugal force is chosen correctly, as shown in Figure 8(b) separation can indeed occur. Here we see that the heavier spheres migrated towards the periphery whilst the lighter ones were held by the gel.

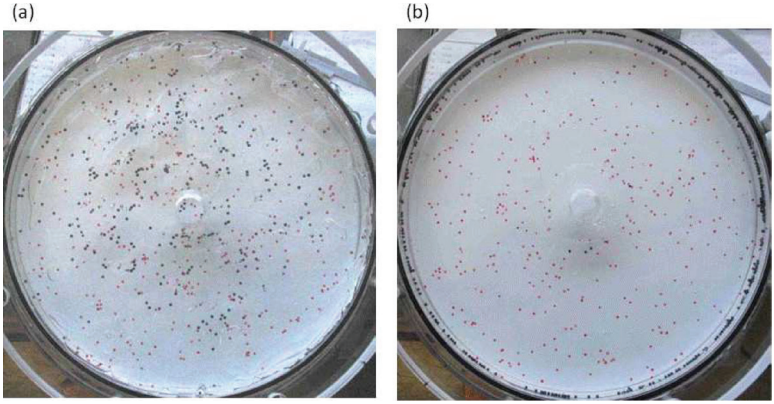

Figure 8. A demonstration of the fractionation of a bidisperse suspension of spherical particles. In (a) an image of the suspension is given before the commencement of the centrifuge. (b) is the state of the suspension after the application of the centrifugal force.It should be noted that most of the darker particles are on the periphery of the centrifuge.

4.2 Cylinders

From the previous subsection, we demonstrated that these gels could be used to create a separation of a bidisperse suspension of spheres. As a proof of principle, we show a nearly perfect separation of a bidisperse suspension of spheres based upon particle density. In this section we continue to build on our understanding of this separation and report on the motion of isolated cylinders in a centrifuge. Cylinders are a more complicated geometry and we suspect that orientation could affect the shape of the unyielded envelope. We present the results in this subsection in a similar manner as to those present in the previous subsection. First the results for isolated particles are given followed by a number of fractionation demonstration experiments.

To begin, like spheres we measured F_c for a large number of cylinders of different aspect ratio, diameter, density, degree of curvature, and orientation (measured relative to the application of force). The results for rigid cylinders are shown in Figure 9. The first observation that can be made is that with increasing aspect ratio, a larger force is required to initiate motion for the cylinders oriented perpendicularly to the direction of force than those oriented in the parallel sense. We report these two bounds as we feel that any orientation state between these two limits should lie somewhere between

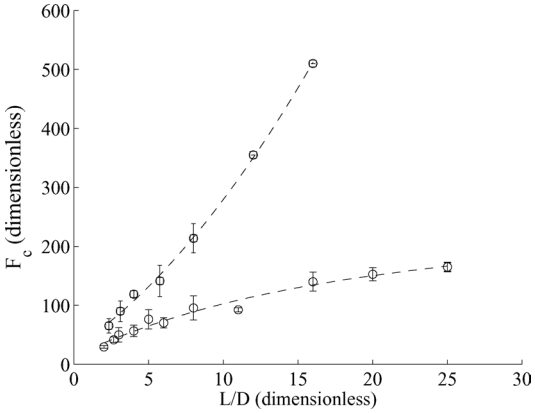

Figure 9. Measurement of the critical force ratio F_c to cause motion in isolated cylinders of various aspect ratios. Cylinders oriented perpendicular to the direction of the force are shown as a square (□). Cylinders oriented with their axis parallel to the direction of force are shown as circles (○). The uncertainty in the estimates are given as a standard deviation.

these two curves. The second observation that we can see is that for cylinders oriented perpendicular to the direction of the force, F_c was found to vary nearly linearly with the aspect ratio of the particle, that is

$$\frac{\Delta\rho V R\omega_c^2}{\tau_y D^2} \approx k_1 \frac{L}{D} \tag{9}$$

where k_1 is the constant of proportionality, and ω_c is the critical velocity in which motion was induced. With this we see that

$$\Delta\rho D \approx \frac{k_1 \tau_y}{R\omega_c^2} \tag{10}$$

It should be noted that the lefthand side of this equation has units of kg/m^2. This is illustrative as this indicates that this separation principle is based upon the mass per unit area. This result is similar to the fractionation principle for settling in Newtonian fluids where we discussed that the terminal velocity was also related to the specific area of the particle; the difference however is that the specific surfaces for each case are defined differently. In addition, this finding indicates that the criteria for motion in this orientation is independent of the length. The separation principle is based solely upon the density and diameter of the cylinder. We feel that this is a significant finding as, in time,

this may imply that a separation mechanism is possible which is independent of length.

The second observation that can be made from Figure 9 is that for particles oriented parallel to the direction of the force, at large aspect ratios, F_c seemingly approaches a constant value. Although we are not completely certain of this point, the physical interpretation of this finding is quite significant in terms of the separation principle. If we set

$$\frac{\Delta\rho V R\omega_c^2}{\tau_y D^2} \approx k_2 \tag{11}$$

where k_2 is the constant of proportionality we see that

$$\Delta\rho L \approx \frac{k_2\tau_y}{R\omega^2} \tag{12}$$

which implies that the separation is independent of particle diameter. To summarize, both Equations 10 and 12 indicate that the separation is based upon the mass per unit area of the cylinder. In one extreme of orientation, the separation is independent on length when oriented perpendicular to the direction of force – in the other extreme it is independent on diameter when oriented parallel to the direction of force (and at large aspect ratios).

At this point we attempt to demonstrate this principle by creating separations based upon either diameter or density. In Figure 10 the cylinders in

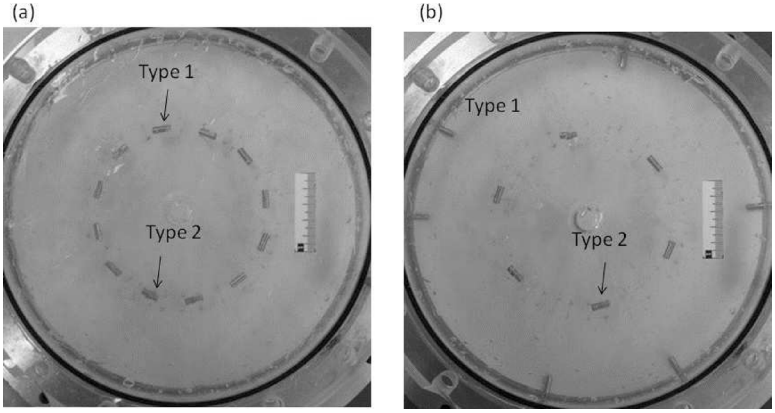

Figure 10. A demonstration of the fractionation of a bidisperse suspension of cylindrical particles.

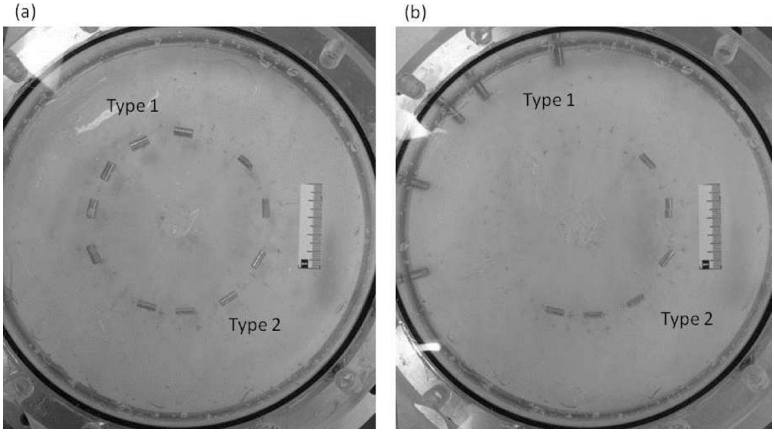

Figure 11. A demonstration of the fractionation of a bidisperse suspension of cylindrical particles.

this case have equal diameter and length but have two different densities. The lighter colored rod has the larger density. In Figure 10(a) an image of the particles is given before the commencement of the centrifuge. In Figure 10(b) the state of the suspension after the application of the centrifugal force is shown. It should be noted that all of the denser particles moved to the periphery while the less dense ones remained trapped. In a similar manner we demonstrate a fractionation based upon diameter. In Figure 11, the cylinders in this case have equal density and length but have two different diameters. The larger diameter rods are located in the upper left quadrant of the image in (a). In (a) an image of the particles is given before the commencement of the centrifuge. (b) is the state of the suspension after the application of the centrifugal force. It should be noted that all of the larger diameter particles moved to the periphery while the smaller diameter ones remained trapped.

With the principle of separation shown for isolated particles, we attempt to perform a demonstration of this principle with particles better representing papermaking fibres. We do so in two separate studies with nylon fibre suspensions of various length and denier[4]. As the density of these particles are so small in comparison to the test particles used, the separation was conducted in the higher speed centrifuge. In the first series of tests, see

[4] Denier is unit of measurement of linear density of textile fiber mass- calculated as one gram per 9000 meters. It is related to diameter of the fibre.

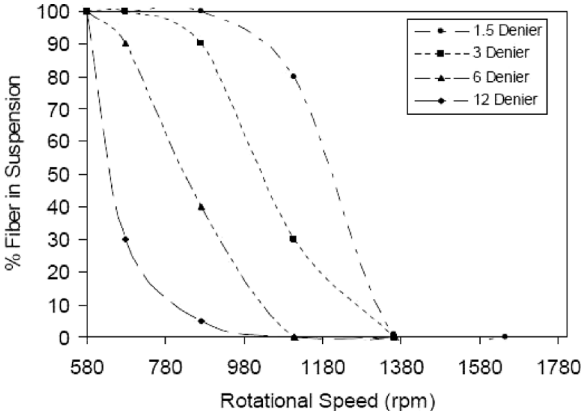

Figure 12. The fraction of nylon particles remaining stably trapped after the application of a centrifugal force. The fibres were randomly oriented initially. The nylon particle were of equal length. Denier is a representation of the diameter of the fibre.

Figure 12, nylon fibre suspensions of various denier were suspended in a Carbopol gel and rotated at increasing rpm. The portion of the fibres which were stably trapped were recovered and the number of fibres determined using a Fibre Quality Analyser (www.optest.com). The orientation of the fibres was not controlled in this experiment and should be considered to be randomly distributed. The results indicate that he threshold required to cause motion increased with increasing denier of the particle. What is evident in this Figure is that a complete separation of say a 1.5 denier particle from a 12 denier particle could be achieved at 980 *rpm*. In the second set of tests, a suspension of equal denier nylon fibres but with different lengths are separated in a centrifuge, see Figure 13. Here nearly complete separation was achieved at 1200 *rpm*.

5 LIMITATIONS – APPLICATIONS TO REAL SYSTEMS

At this point we are trying to build an understanding of the limitations of the proposed separation principle. Thus far we have studied ideal systems both in terms of the definition of the properties of the particles and in terms of the concentration regimes tested, i.e. dilute. A small discussion of each is given below.

We begin to test the assumption regarding the shape of papermaking fibres

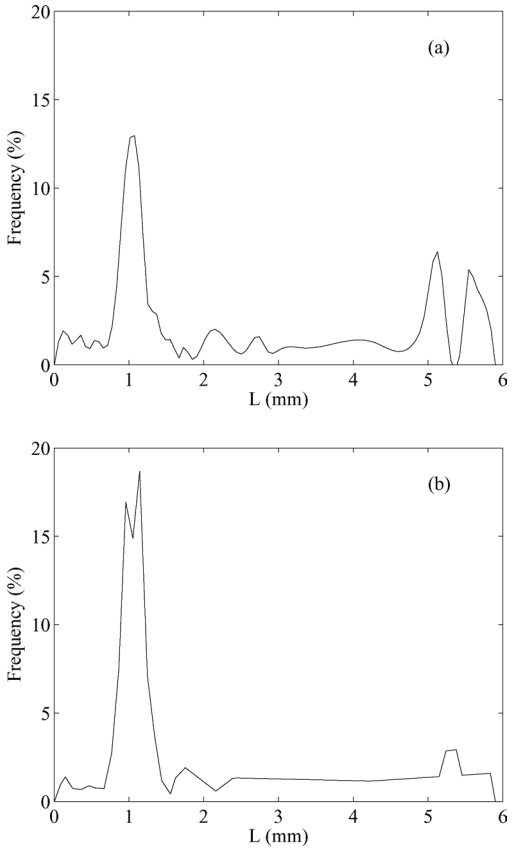

Figure 13. The separation of Nylon fibres with equal diameters but different lengths. (a) The fibre length distribution of the sample initially. (b) The fibre length distribution of the stably trapped fibres after treatment with the centrifuge at 1200 *rpm*.

by including the effects of kink or curl into the particle. To do so we modified our system by bending the cylindrical rods and then measuring F_c in the manner described above, see Figure 14. What is evident is that F_c is quite sensitive to the bend in the rod. This will need to be addressed in further work.

In addition, the size of the unyielded envelope places an upper limit on the concentration of the suspension which can be used. Here, the separation principle will be diminished if the unyielded zones of adjacent particles

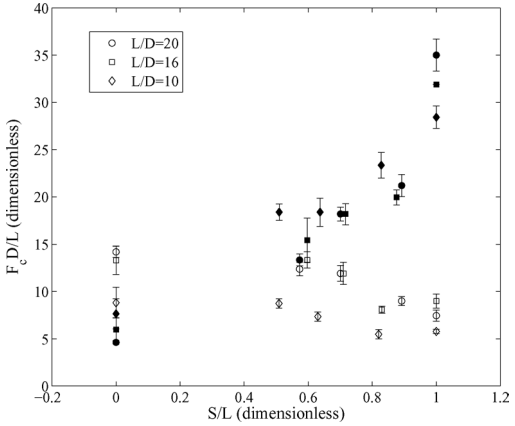

Figure 14. Measurement of the critical force ratio F_c to cause motion in isolated bent cylinders. The measurements were conducted both as function of aspect ratio and degree of kink S/L. Particles oriented perpendicular to the direction of force is shown as filled symbols. Particles oriented parallel to the direction of force are unfilled symbols.

overlap. Just like with particle flow with Newtonian fluids, this represents a long-range hydrodynamic disturbance. At this point we attempt to estimate the size of the unyielded zone based upon our experimental results. To do so we conducted a series of tests where spheres of a known diameter which were placed at equal R in the centrifuge but at different interparticle spacings. The isolated particle results could be obtained when the interparticle spacing was greater than one particle diameter.

6 SUMMARY AND CONCLUSIONS

In this work we advanced the argument of a novel separation principle. Here we propose that the separation principle is based upon controlling the threshold for motion of individual classes of particles. If the threshold can be controlled to a high enough resolution then in principle any separation could be achieved. In this work we set our threshold by the balance between the centrifugal force and the yield stress of a gel. Other systems could be used to control this to a finer scale.

This principle is strikingly different than that used in present industrial or even laboratory devices. Here, the separation is based upon the difference in the terminal velocities of the particle which is related to parameters such as

density and specific surface. The efficiency of this separation is diminished due to long-range hydrodynamic interactions.

We have demonstrated under very ideal conditions that separation can indeed be achieved with these types of gels. We found out that with rods the separation is based upon the mass per unit area of the particle and orientation has a large effect on stability. It was shown that when the cylinders were oriented perpendicularly to the direction of the force, the threshold for motion is independent of length. Similarly, when oriented parallel to the direction of force, the threshold is independent of diameter. Simple test cases were performed with nylon fibre suspensions in which separation was achieved based upon either length or diameter.

Finally, we argued that there are limitations to this proposed system before its reduction into practice. First, this system too is limited by the long range hydrodynamic interactions. However, the interactions are on a smaller scale and limited to the interaction length created by the unyielded envelope. In addition, we see that the separation is based upon the mass per unit area of the unyieded envelope. The size and shape of the unyield envelope is still an open question in the literature. Understanding this will allow for an estimate of the upper limit of the efficiency of this proposed separation technique in terms of concentration and classes of particles which can be separated from each other.

ACKNOWLEDGMENTS

We gratefully acknowledge financial support of the Natural Sciences and Engineering Research Council of Canada through the Collaborative Research and Development program and through the support of our partners BC Hydro, Paprican, Catalyst Papers, Howe Sound Pulp and Paper, West Fraser Quesnel River Pulp, Canfor, Andritz, Arkema, Honeywell, WestCan Engineering, Advanced Fiber Technologies, Ontario Power Authority and CEATI international. In addition D.M. Martinez would like to thank Dr Daniel Ouellet and Mr John Senger for many fruitful discussions in the initial part of this work.

REFERENCES

1. Sloane, C.M. 2000 Kraft pulp processing – pressure screen fractionation *Appita J.* **53(3)**, 220–226.
2. Julien Saint Amand, F., & Perrin, B. 1999 Fundamentals of screening: effect of rotor design and fibre properties *Tappi Pulping Conf*, 941–945.

3. Olson J.A. Allison, B.J. Friesen, T. & Peters, C. 1999 Fibre fractionation for high-porosity sack kraft paper. *Papricon Pulp and Paper Report* 1432.
4. Olson J.A., Allison B.J. & Roberts N. 2000 Fibre length fractionation caused by pulp screening. Smooth-hole screen plates *J. Pulp Paper Sci.* **26(1)**, 12–16.
5. Olson J.A. 2001 Fibre length fractionation caused by pulp screening, slotted screen plates *J. Pulp Paper Sci.* **27(8)**, 255–261.
6. Paavilainen, L. 1992 The possibility of fractionating softwood sulfate pulp according to cell wall thickness *Appita J.* **45(5)**, 319–326.
7. Vomhoff H. & Grundström, K.J. 2003 Fractionation of a bleached softwood pulp and separate refining of the earlywood andlatewood enriched fractionation *Das Papier* **2**, 37.
8. Batchelor, G.K. 1972 Sedimentation in a dilute dispersion of spheres *J. Fluid Mech.* **123**, 245–268.
9. Mackaplow, M.B. & Shaqfeh, E.S.G 1998 A numerical study of the sedimentation of fibre suspensions *J. Fluid Mech.* **376**, 149–182.
10. Jayaweera, K.O.L.F. & Mason, B.J. 1965 The behaviour of freely falling cylinders and cones in a viscous fluid *J. Fluid Mech.* **22**, 709–720.
11. Happel, J. & Brenner, H. 1965 Low Reynolds Mumber Hydrodynamics *Prentice-Hall*.
12. Kumar, P. & Ramarao, B.V. 1991 Enhancement of the sedimentation rates of fibrous suspensions *Chem. Engng. Comm.* **108**, 381–401.
13. Herzhaft, B. & Guazzelli, E. 1999 Experimental study of the sedimentation of dilute and semi-dilute suspensions of fibres *J. Fluid Mech.* **384**, 133–158.
14. Richardson J. F. & Zaki W. N. 1954 Sedimentation and fluidisation, Part.1 *Trans. Instn Chem. Engrs.* **(32)**, 35–53.
15. Butler, J.E. & Shaqfeh, E.S.G 1989 Dynamic simulations of inhomogeneous sedimentation of reigid fibres *J. Fluid Mech.* **468**, 205–237.
16. Koch, D.L. & Shaqfeh, E.S.G 1989 The instability of a dispersion of a dispersion of settling spheroids *J. Fluid Mech.* **224**, 275–303.
17. Marton, R. & Robie, J.D. 1969 Characterization of mechanical pulps by a settling technique *TAPPI J.* **22(12)**, 2400–2406.
18. Feng, J. Hu, H.H. & Joseph, D.D. 1998 Direct simulation of initial value problems for the motion of solid bodies in a Newtonian fluid Part 1. Sedimentation *J. Fluid Mech.* **261**, 95–134.
19. Jianzhong, L., Xing, S. & Zhenjiang, Y. 2003 Effects of the aspect ratio on the sedimentation of a fiber in Newtonian fluids *J. Aer. Sci.* **34**, 909–921.
20. Holm, R. Storey, S. Martinez, D.M & Söderberg, D. 2004 Visualization the motion of settling dilute rigid fibre suspensions *Progress in Paper Physics* Trondheim Norway.
21. Salmela, J. Martinez, D.M. & Kataja, M. 2007 Sedimentation of dilute and semi-dilute rigid fibre suspensions at finite Re *AIChE J.* **53(8)**, 1916–1923.
22. Ko, J. 2005 Numerical modeling of highly swirling flows in a cylindrical through Flow hydrocyclone *Licentiate Thesis* **KTH** Sweden
23. Narashima M., Brennan M., & Holtham P.N. 2007 Review of CFD modelling

for performance prediction of hydrocyclones *Engineering Applications of Computational Fluid Mechanics* **1(2)**, 109–125.
24. Nowakowski, A. F. & Dyakowski, T. 2003 Investigation of swirling flow structure in hydrocyclones *Trans IChemE* **81(A)**, 862–874.
25. Bergstrom J. & Vomhoff H. (2007) Experimental hydrocyclone flow field studies *Separation and Purification Technology* **53(1)**, 8–20.
26. Hsieh, K. T. & Rajamani, R. K. 1991 Mathematical model of the hydrocyclone based on physics of fluid flow *AIChE J.* **37(5)**, 735–746.
27. Sevilla, E. M. & Branion, R. M. R. 1997 The fluid dynamics of hydrocyclones *J. Pulp Pap. Sci.* **23(2)**, 85–93.
28. Boysan, F. Ayres, W. H. & Swithenbank, J. 1982 A fundamental mathematic modeling approach to cyclone design *Trans IChemE* **60**, 222–230.
29. Ma, L., Ingham, D. B. & Wen, X. 2000 Numerical modeling of the fluid and particle penetration through sampling cyclones *J. Aer. Sci.* **31(9)**, 1097–1119.
30. Andres U. T. 1961 Equilibrium and motion of spheres in a viscoplastic liquid *Sov. Phys. Doklady (U.S.A.)* **5**, 723–730.
31. Blackery, J. & Mitsoulis, E. 1997 Creeping motion of a sphere in tubes filled with a Bingham plastic material *J. Non-Newtonian Fluid Mech.* **70**, 59–77.
32. Liu, B.T. Muller, S.J. & Denn, M. 2002 Convergence of a regularization method for creeping flow of a Bingham material around a rigid sphere *J. Non-Newtonian Fluid Mech.* **102**, 179–191.
33. Beaulne, M. & Mitsoulis, E. 1997 Creeping motion of a sphere in tubes filled with Herschel-Bulkley fluids *J. Non-Newtonian Fluid Mech.* **72**, 55–71.
34. Jie, P. & Zhu, K.-Q. 2006 Drag force of interacting coaxial spheres in viscoplastic *J. Non-Newtonian Fluid Mech.* **135**, 83–91.
35. Frigaard, I.A. & Nouar, C. 2005 On the usage of viscosity regularisation methods for visco-plastic fluid flow computation *J. Non-Newtonian Fluid Mech.* **127**, 1–26.
36. Beris, A.N. Tsamopoulos, J.A. Armstrong, R.C. & Brown, R.A. 1985 Creeping motion of a sphere through a Bigham plastic *J. Fluid Mech.* **158**, 219–244.
37. Putz, A. Burghelea, T. Frigaard, I.A. & Martinez, D.M. 2008 Settling of an isolated spherical particle in a yield stress fluid *Phys. Fluids* **20(3)**, 033102–033102,11.
38. Tabuteau, H. Coussot, P. & de Bruyn, J.R. 2007 Drag force on a sphere in steady motion through a yield stress fluid *J. Rheol.* **51**, 125–137.
39. Laxton, P.B. & Berg J.C. 2005 Gel trapping of dense colloids *J. Colloid Interface Sci* **285**, 152–157.
40. Glowiniski. R. & Le Tallek, P. 1987 "Augmented lagrangian and operator splitting methods in non-linear mechanics" *Studies in Applied and Numerical Mathematics* (Society for Industrial & Applied Mathematics, Philedelphia)
41. Fortin, M. & Glowiniski, R. 1983 "Augmented lagranian methods" (North Hoilland, Amsterdam)
42. Roquet, N. & Saramito, P. 1983 An adaptive finite element method for Bingham fluid flows around a cylinder *Comput. Methods Appl. Mech. Eng.* **192**, 3317–3341.

43. Chhabra R.P. 2007 "Bubbles, drops and particles in non-newtonian fluids" (CRC, Boca Raton, Fl)
44. Gueslin, B., Talini, L., Herzhaft, B., Peysson, Y. & Allain, C. 2006 Aggregation behavior of two spheres falling through an aging fluid *Phys. Rev.* **74**, 042501.
45. Attapatu, D.D. Chhabra R.P & Uhlherr, J. 1995 Creeping sphere motion in Herschel-Bulkley fluids: Flow field and drag *J. Non-Newtonian Fluid Mech.* **59**, 245–265.
46. Jossic L. & Magnin A 2001 Drags and stability of objects in a yield stress fluid *AIChE J.* **47**, 2666–2672.

A EXPERIMENTAL CONDITIONS

Table 1. The experimental conditions for determination of F_c for spherical particles. The spheres in this case all had a density of 7800 kg/m^3. N represents the number of replicates and the uncertainty in F_c is reported at the 95% confidence interval

D (*mm*)	τ_y (*Pa*)	N	F_c (*dimensionless*)
2.4	0.9	70	29.0(±0.7)
2.4	3.1	200	24.0(±1.0)
3.2	0.9	150	23.0(±1.3)
3.2	3.3	150	20.3(±0.4)
4.0	3.1	75	17.4(±0.3)
4.0	3.3	170	17.3(±0.3)
4.8	3.1	150	14.8(±0.3)
4.8	3.3	170	14.4(±0.2)
5.6	3.1	70	13.6(±0.5)
5.6	3.3	130	13.2(±0.3)

Table 2. The experimental conditions for determination of F_c for cylindrical rods with their axes oriented normal to the direction of force. N represents the number of replicates and the uncertainty in F_c is reported at the 95% confidence interval

τ_y (*Pa*)	ρ (*kg/m³*)	D (*mm*)	L/D	N	F_c (*dimensionless*)
3.3	7800	1.6	6.0	90	190(±3)
3.3	7800	1.6	12.0	50	372(±9)
3.3	7800	1.6	16.0	55	517(±17)
3.3	7800	2.4	2.6	110	83(±1)
3.3	7800	1.6	4.0	100	127(±2)
3.3	7800	3.2	2.0	90	50(±1)
3.3	7800	3.2	3.0	120	90(±2)
3.3	7800	3.2	4.0	95	118(±3)
3.3	7800	4.8	2.0	90	62(±1)
4.0	8300	1.6	4.0	80	115(±2)
4.0	8300	1.6	6.0	75	179(±4)
4.0	8300	1.6	8.0	75	237(±5)
4.0	8300	3.2	3.0	60	81(±2)
4.0	8300	3.2	4.0	75	124(±3)
4.0	8300	3.2	5.0	75	145(±4)
4.0	8300	3.2	6.0	90	174(±5)
4.0	8300	4.8	2.6	85	77(±2)
4.0	8300	4.8	3.3	65	107(±3)
4.0	8300	4.8	4.0	70	114(±4)

Table 3. The experimental conditions for determination of F_c for cylindrical rods with their axes oriented normal to the direction of force. N represents the number of replicates and the uncertainty in F_c is reported at the 95% confidence interval

τ_y (Pa)	ρ (kg/m^3)	D (mm)	L/D	N	F_c
4.0	2700	0.4	16.0	50	183(±5)
4.0	2700	0.4	20.0	50	169(±6)
4.0	2700	0.4	28.0	30	214(±5)
4.0	7800	1.6	4.0	85	49(±2)
4.0	7800	1.6	6.0	75	59(±2)
4.0	7800	1.6	8.0	80	67(±3)
4.0	7800	1.6	12.0	90	96(±3)
4.0	7800	1.6	16.0	70	128(±6)
4.0	7800	1.6	20.0	90	170(±12)
4.0	7800	1.6	25.0	55	165(±7)
4.0	7800	2.4	2.6	70	37(±1)
4.0	7800	2.4	4.0	80	52(±2)
4.0	7800	2.4	6.6	95	80(±3)
4.0	7800	2.4	8.0	95	111(±4)
4.0	7800	2.4	10.6	65	92(±2)
4.0	7800	3.2	2.0	100	28(±1)
4.0	7800	3.2	3.0	120	43(±2)
4.0	7800	3.2	4.0	100	51(±3)
4.0	7800	3.2	6.0	80	79(±3)
4.0	7800	3.2	8.0	65	103(±4)
4.0	7800	4.8	2.0	80	33(±1)
4.0	7800	4.8	2.6	80	41(±2)
4.0	7800	4.8	3.3	70	51(±2)
4.0	7800	4.8	4.0	65	57(±2)
4.0	8300	1.6	4.0	90	60(±2)
4.0	8300	1.6	6.0	100	83(±2)
4.0	8300	1.6	8.0	100	114(±3)
4.0	8300	3.2	3.0	80	47(±1)
4.0	8300	3.2	4.0	80	66(±2)
4.0	8300	3.2	5.0	100	70(±2)
4.0	8300	3.2	6.0	90	75(±4)
4.0	8300	4.8	2.6	90	90(±2)
4.0	8300	4.8	3.3	80	65(±2)
4.0	8300	4.8	4.0	75	75(±2)

Table 4. The experimental conditions for determination of F_c for bent cylindrical rods with their axes oriented normal to the direction of force, see Figure 5. In this case the density of the fibres were 7800 kg/m^3, τ_y = 5.3 *Pa*, and D = 0.4 *mm*. N represents the number of replicates and the uncertainty in F_c is reported at the 95% confidence interval

L/D	S/L	N	F_c
10	0.51	20	183(±8)
10	0.70	20	183(±14)
10	0.89	20	233(±14)
16	0.59	30	244(±37)
16	0.71	30	290(±17)
16	0.83	30	319(±12)
20	0.50	60	267(±12)
20	0.63	60	363(±14)
20	0.82	60	423(±23)

Table 5. The experimental conditions for determination of F_c for bent cylindrical rods with their axes oriented parallel to the direction of force, see Figure 5. In this case the density of the fibres were 7800 kg/m^3, τ_y = 5.3 *Pa*, and D = 0.4 *mm*. N represents the number of replicates and the uncertainty in Y_c is reported at the 95% confidence interval

L/D	S/L	N	F_c
10	0.51	60	139(±5)
10	0.63	60	117(±4)
10	0.82	60	87(±4)
16	0.59	50	213(±5)
16	0.71	50	190(±6)
16	0.83	50	129(±4)
20	0.57	50	247(±5)
20	0.07	55	238(±6)
20	0.89	40	220(±5)

Transcription of Discussion

NOVEL FRACTIONATION METHODS: SEPARATION IN A VISCOPLASTIC FLUID

A. Madani,[1] *S. Storey*,[1] *J.A. Olson*,[1] *I.A. Frigaard*,[1] *J. Salmela*[2] and *D.M. Martinez*[3]

[1]Dept. of Mechanical Engineering, The University of British Columbia, 2324 Main Mall, Vancouver BC, V6T 1Z4, Canada
[2]VTT, P.O. Box 1603, FIN-40101, Jyväskylä, Finland
[3]Dept. of Chemical and Biological Engineering, The University of British Columbia, 360 East Mall, Vancouver, BC, V6T 1Z3, Canada

Steve Keller Miami University

At what concentration of particles do you see the volume displacement of fluid going in the reverse direction begin to affect your results?

Mark Martinez

You mean in a Newtonian fluid?

Steve Keller

Yes.

Mark Martinez

There was a crowding number of about 5; that is a "handsheet concentration" – 0.2 %. To answer your question, the fluid flow affects the results at all concentration regimes.

Discussion

Warren Batchelor Monash University (from the chair)

Do you have any good way of being able to recover the fluid which you use in these separations?

Mark Martinez

Not at this point. This is just a demonstration of the principle.

Daniel Söderberg KTH / Innventia

This is a novel principle – what would be the concentration limits?

Mark Martinez

Our student is working on this. He is currently doing the separations at about 0.5% consistency.

Daniel Söderberg

I imagine that, in this type of centrifuge separation, large particles moving through the fluid would eventually capture small particles and drag them along?

Mark Martinez

Sure, by all means. What is interesting too is the concept of the yield stress. I thought this would be the ultimate limitation of the process. There's a fundamental understanding I don't have about figure 3 in the paper: what creates the yield surface? What are the kinetics of a yield surface forming and melting? If this was an instantaneous process, then you'd be right: if one particle came into the envelope of another particle, then they would form a larger envelope and continue together and that would be the ultimate limit on concentration. But we did that in the lab and we could see one particle going into the envelope of another particle and pushing it out of the way, and moving past. So there is something about the kinetics of the formation of these envelopes and their coalescence which we don't understand.

Stefan Lindström Mid Sweden University

This method may create another problem when you later try to displace the elastic fluid, because you have to remove it when you are going to use the fibres later. Have you thought about this yet?

Mark Martinez

Clearly, yes there is a problem, but some fluids with these viscoelastic (rather than elastic) properties are already in the paper making process. Also, for this one type of fluid, you can destroy the gel in a number of different ways: using pH or using sound, for example. Don't forget this is a demonstration experiment and not an industrial process.